Noname manuscript No.
(will be inserted by the editor)

A 120 GHz QVCO with 16.2 GHz Tuning Range Resistent Against VCO Pulling in 45 nm CMOS

the date of receipt and acceptance should be inserted later

Abstract Frequency pulling of an oscillator integrated in a quadrature phase-shift keying (QPSK) wireless transmitter degrades the performance of the wireless system. This paper analyses the behavior of an oscillator in the presence of coupling between the oscillator and a power amplifier or antenna. Symbol switching in the modulator will cause frequency shifts in the oscillator at the modulation frequency. A new architecture for a 120 GHz quadrature frequency generator with large tuning range and immunity against PA-VCO coupling is presented. Combining the output signals of two independent oscillators, the pulling effect is removed and the frequency generator can be integrated with a PA and an antenna on the same chip. This architecture also makes quadrature generation with large tuning range feasible at 120 GHz. The chip is fabricated in a 45 nm CMOS technology and shows a tuning range of 16.2 GHz (13.5 %), a phase noise of -112 dBc/Hz @ 10 MHz offset and a phase error of 5 ° [1].

Keywords Pulling · Quadrature VCO · Tuning range · CMOS · Mm-wave

1 Introduction

Highly integrated millimeter-wave CMOS circuits for high data rate wireless communication systems have emerged in recent years. These systems certainly benefit from the high bandwidth that is available at mm-wave frequencies and thus can achieve high data rates even with simple modulation schemes. But nevertheless, also these systems are now evolving towards more complex quadrature modulation schemes like QPSK and QAM [2] [3] and thus require a quadrature mm-wave local oscillator (LO). Due to the small wavelengths, the integration of antennas on a silicon chip becomes feasible at these high frequencies [3] [4]. However, integrating both an oscillator and a transmitter with an antenna on the same chip increases the coupling between the power amplifier and the antenna, back to the oscillator (Fig. 1). Different coupling mechanisms exist [5]. The two main mechanisms are resistive coupling through the substrate and magnetic coupling between the inductor of the VCO and the on-chip antenna. This coupling can lead to injection locking or spurious mixing products to appear in the output spectrum, but to reach very high data rates, a constellation with a good error vector magnitude (EVM) needs to be generated in the transmitter and thus a spectral pure LO signal is required. Therefore it is important to understand this LO pulling behavior. First Adler [6] and later Razavi [7] studied injection locking of oscillators under the injection of an external signal and an expression was found for the locking range. In a direct conversion transmitter the injected signal has the same frequency as the oscilator and thus falls within the locking range. Hsiao [8] described frequency pulling of a phase locked oscillator in such a transmitter and gave a solution to reduce its influence on the performance of the system. However, because of its complexity, the presented technique is not applicable to a mm-wave free-running oscillator.

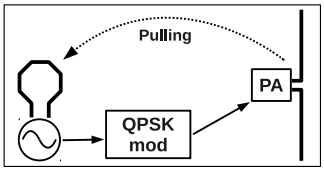

Fig. 1 QPSK transmitter with on-chip antenna causing VCO pulling.

Eliminating frequency pulling is not the only challenge when designing a mm-wave quadrature oscillator. Also a large tuning range is necessary to overcome process variations and the uncertainty of the transistor models at these

Address(es) of author(s) should be given

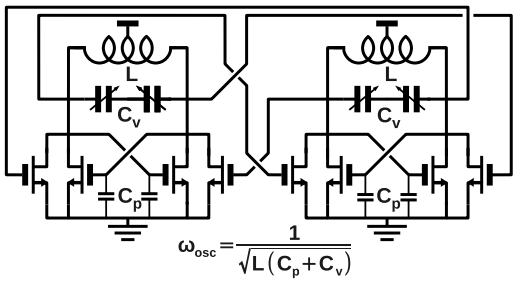

Fig. 2 Conventional fundamental quadrature VCO.

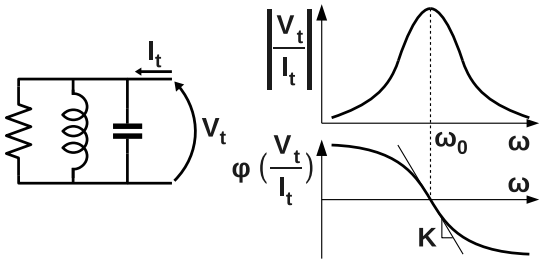

Fig. 3 The resonant tank of a cross-coupled oscillator and the magnitude and phase characteristic of its impedance

high frequencies. In a fundamental mm-wave VCO, a large tuning range is difficult to achieve due to the large portion of parasitic capacitance and inductance in the resonant LC tank. Furthermore, conventional quadrature VCOs utilize coupling transistors to force 90 degrees phase difference between two oscillators (Fig. 2). These coupling transistors are indeed an extra load on the LC-tank which makes it more difficult to sustain an oscillation with the limited device gain at mm-wave frequencies and to combine this with a large tuning range.

In section 2.1 VCO injection locking is examined and in section 2.2 LO pulling in a QPSK transmitter is graphically explained. The proposed architecture is presented in Section 3 and the implementation in Section 4. Section 5 gives the measurement results.

2 VCO coupling behavior

This section starts with a general description of injection locking in LC oscillators. To simplify the analysis, the parasitic capacitances and inductances in the oscillator are neglected. Measurements were performed to verify this locking behavior when an integrated transmitter acts as interferer. Also the injected power into the VCO by the PA is calculated. The second subsection will give insight in the LO pulling behavior when a QVCO drives a QPSK transmitter on the same chip.

2.1 Injection locking

Figure 3 shows a parallel resonant tank which is often used in cross-coupled LC oscillators. The magnitude and phase characteristic of the impedance of the tank are also given. The oscillation frequency of a harmonic oscillator is determined by the inductance and capacitance in the resonator. At this frequency the phase shift in the tank is zero and oscillation is possible. When this LC circuit operates at another frequency than its resonant frequency, there will be a phase shift between the voltage V_t and the current I_t. The parallel resistor represents the loss in the LC-tank and is related with the width of the resonant peak in the magnitude plot and with the slope (K) at the zero crossing in the phase plot. A lower loss in the resonant tank increases the slope (K) of the phase characteristic and leads to a smaller frequency deviation for some phase shift. The circuit in fig. 3 can not oscillate without compensating the loss of the LC-tank. To fullfil the Barkhausen stability criterion, not only does the phase shift across the tank needs to be zero, also the loop gain needs to be equal to one. Therefore a gain stage, represented by a negative resistor which injects the same amount of energy as is lost in the tank, is added in fig. 4. In this way a steady state oscillation is achieved. When no other signals are injected into the oscillator ($I_p = 0$), the current I_c is in phase with I_t and equally large. Locking the oscillator to a frequency different from ω_0 with an injected signal I_p results in a phase shift $\Delta\varphi$ in the LC-tank (between V_t and I_t). Since I_c is still in phase with V_t, I_c has to form an angle $\Delta\theta$ with I_p to fullfil Kirchhoff's current law. Increasing the gap between the frequency of the injected signal and the resonance frequency of the LC-tank the angle $\Delta\varphi$ also increases. The maximum value for the angle $\Delta\varphi$ is derived by Razavi [7] and for small injection levels ($I_p \ll I_c$) the locking range is found to be

$$\omega_L \approx \frac{\omega_0}{2Q_{tank}} \frac{I_p}{I_c} \tag{1}$$

Measurements were performed to find the locking range of a 120GHz free-running VCO when the interferer is an on-chip transmitter. Based on the measured locking range and equation 1 the strenght of the injected signal in the VCO can be estimated. For the measurements the chip shown in fig. 5 is used. The circuit on the left-hand side is a 118 GHz VCO with 7.8% tuning range [9]. The other circuit is a 120 GHz 10 Gb/s phase modulating transmitter [10].

To measure the coupling from the transmitter to the VCO, the setup of fig. 6 is used. The output of the periodic signal generator (PSG) is upconverted by an F-band OML source module with 0Bm output power and brought on-chip by a GSG probe. This input signal is amplified in the transmitter and couples into the oscillator through the substrate. The

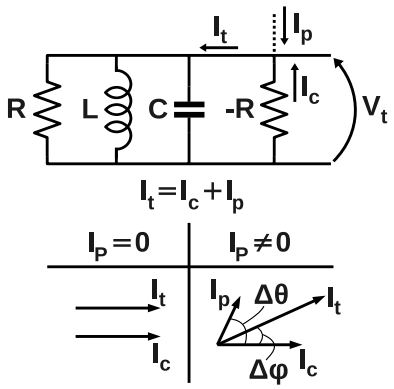

Fig. 4 The simplified schematic of a cross-coupled oscillator and the vector relationship of the currents in the circuit influenced by an external signal I_p

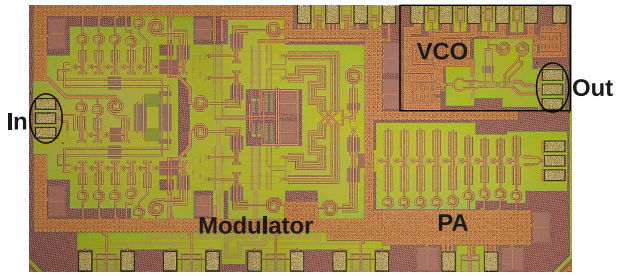

Fig. 5 Die photograph of a VCO [9] and a phase modulation transmitter with PA [10], used to measure injection locking of a mm-wave VCO. The input and output used in this measurement are indicated

Fig. 6 Setup to measure the injection locking of a VCO by a transmitter. The input signal is generated by a PSG, upconverted by an OML source module and brought on-chip by a GSG probe. The output of the VCO is probed, downconverted by a sub-harmonic mixer and displayed on a FSU spectrum analyzer

output of the VCO is probed and downconverted by a sub-harmonic mixer. The LO of the mixer is provided by a signal generator and the IF-output is analysed on a FSU spectrum analyzer. The frequency of the input of the transmitter (the interferer) is sweeped and the locking range is found. The result is shown in fig. 7. Figures 7a and 7c show the oscillator in quasi-lock as described in [7]. On figure 7b the oscillator is in locked state. The spectral purity of the signal of the VCO is improved, which proves the locking. The locking range is 231 MHz when the free-running frequency of the oscillator is tuned to 115 GHz. Now the injected power P_{inj} in the VCO can be calculated using equation 1 and the simulated values in table 1.

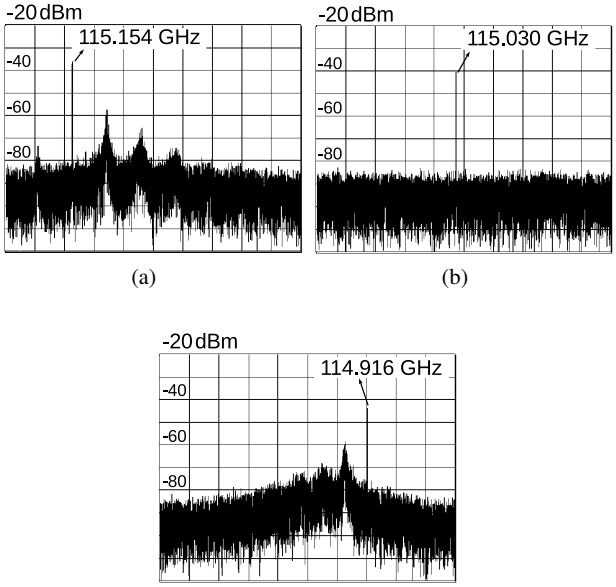

Fig. 7 Measured spectra of the output of the VCO [9] when influenced by an on-chip PA [10]. The output signal is downconverted with a 118 GHz LO. The center frequency and span of the spectra are 115.017 GHz and 500 MHz respectively. Three cases are shown: (a) quasi-lock, (b) locked and (c) quasi-lock.

$$I_p \approx \frac{\omega_L}{\omega_0} 2 Q_{tank} I_c \approx 19\mu A \tag{2}$$

$$P_{inj} \approx \frac{I_p^2}{2} R_{tank} \approx 0.085\mu W \approx -40.7 dBm \tag{3}$$

Table 1 Simulated parameters of the LC-tank of the oscilator

R_{tank}	470Ω
Q_{tank}	8.3
I_c	$0.58mA$

2.2 QPSK LO Pulling

In communication systems, the oscillator is integrated with a quadrature modulator, power amplifier and antenna on the same chip (Fig. 1). This integration results in coupling from the PA and the antenna to the oscillator. The frequency of the pulling signal is equal to the oscillation frequency and thus always falls within the locking range. Figure 8 shows what happens in the oscillator during QPSK switching in the modulator. For the clearness of the figure, the injected signal I_p and the signal from the gain stage I_c have a similar amplitude. However, in the previous section is shown that I_p is

much smaller than I_c. In this example the phase difference $\Delta\theta$ between I_c and I_p is X^o for the first case on the left. This results in a phase shift $\Delta\varphi$ of Y^o. As a consequence, the oscillator will run at a frequency $\omega_0 - Y/K$ where $K(^o/GHz)$ is the linearised slope of the phase characteristic of the resonant tank (see fig. 3). An oscillator with a higher quality LC-tank will experience a smaller frequency shift for the same phase shift. In the second case $\Delta\theta$ is 90^o larger due to a symbol switch in the modulator. As a result, $\Delta\varphi$ is also larger and the oscillation frequency will change. The same is true for the other two cases shown. The oscillation amplitude will also vary during the switching. The reasons are a changing amplitude of the current I_t in the LC-tank and of the impedance of the tank under influence of a frequency shift (as depicted in fig. 3).
Hsiao [11] derived a formula for the instantaneous VCO frequency under directly modulated self-injection

$$\omega_{LO}(t) = \omega_{osc}(t)(1 - \frac{1}{2Q}\frac{I_p(t)}{I_c}sin(\alpha(t))) \tag{4}$$

$$\tag{5}$$

As an example, using the numbers from table 1 and the calculated injected signal $I_p = 19\mu A$, frequency jumps larger than 100MHz are possible. A simulation is performed in which the output of the QPSK modulator is injected into the VCO with a voltage controlled current source to simulate the QPSK pulling behavior. Figure 9 shows the transient results of the output frequency and amplitude of the VCO. As explained in fig. 8 every symbol switch in the QPSK modulator causes frequency shifts because of a changing phase shift and amplitude variations because of a changing amplitude of the tank current I_t and tank impedance. Both effects will cause a severe degradation of the spectral purity of the LO and have a large impact on the performance of a wireless transceiver. Because of the changing LO-frequency caused by a symbol switch, the constellation diagram of the quadrature modulation rotates and the speed and direction of rotation is dependent on the transmitted symbol. For a data rate of 1Gbps and 100MHz frequency jumps the constellation rotates 10% or 36^o during 1 symbol period. To prevent this, the proposed architecture, described in the next section, is used.

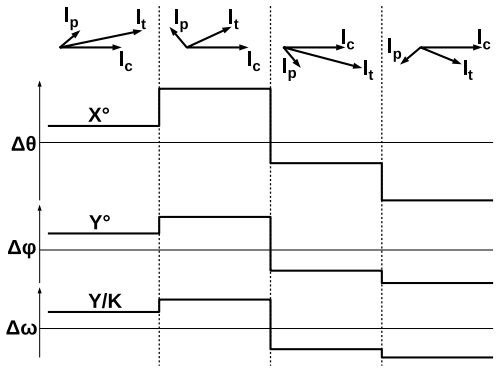

Fig. 8 The vector diagrams and corresponding angles and frequency shifts for the four posible symbols in the QPSK modulator

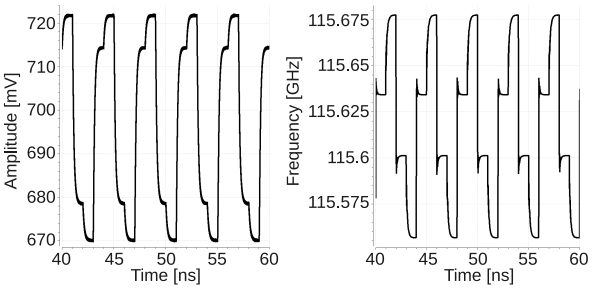

Fig. 9 The amplitude and frequency variatons of the output signal of the oscillator during QPSK switching in the modulator

3 120GHz QVCO insensitive to injection locking

The proposed architecture of the 120 GHz quadrature signal generator is shown in fig. 10a. Two coupled 48 GHz oscillators (hereinafter referred to as "VCO1") generate the four quadrature phases. The outputs of the quadrature oscillators and a 72 GHz oscillator ("VCO2") are multiplied to produce the 120 GHz quadrature signals. Differential buffers are placed between the oscillators and the mixers to avoid extra loading on the LC-tank of the oscillators. A large tuning range is achieved by controlling the frequency of both VCO1 and VCO2 and by making a combination of digital tuning (b_{0-3} and b_{4-5}) and analog tuning (V_{ctrl}). Due to the lower oscillation frequencies of both oscillators, a larger variable capacitance can be tolerated, which results in a larger tuning range. By mixing the output of two oscillators of which the phase noise is uncorrelated, a 3 dB phase noise improvement is achieved compared to a 60 GHz doubler. For example, two 60 GHz uncorrelated sources with a phase noise of -90 dBc/Hz translate after mixing to a 120 GHz signal with a phase noise of -87 dBc/Hz. Doubling the same 60 GHz source will generate a 120GHz signal with a phase noise of -84 dBc/Hz. The proposed solution uses two different oscillator architectures and the output phase noise will be dominated by the VCO with the largest phase noise, but still perform better than using a frequency multiplier.
At the outputs of the two mixers, signal splitters and switchable buffers provide the ability to drive two isolated outputs with differential I/Q signals, e.g. for both a transmitter and a receiver. For measuring purposes one output is connected to a GSG probepad while the other quadrature outputs are downconverted by an on-chip mixer and baseband amplifier to measure the quadrature accuracy. The key advantage of this architecture is the signal generation at lower frequencies, which enables quadrature generation and large

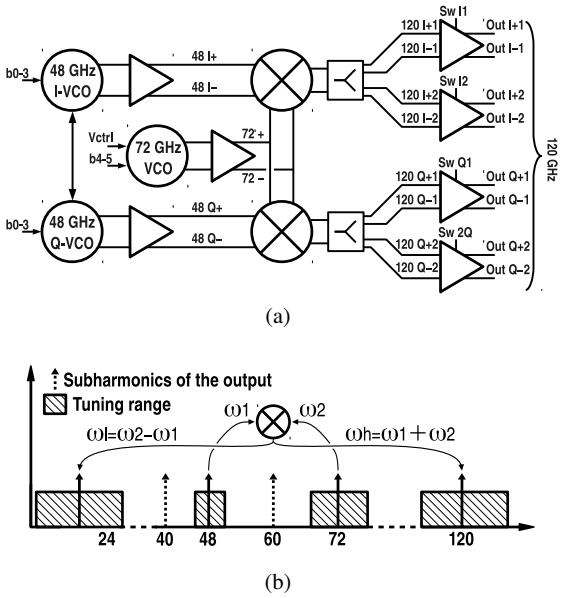

Fig. 10 (a) The proposed architecture of the 120 GHz VCO containing two coupled 48 GHz VCOs, a 72 GHz VCO, two mixers, two output splitters and buffers and (b) overview of the frequency locations in the system

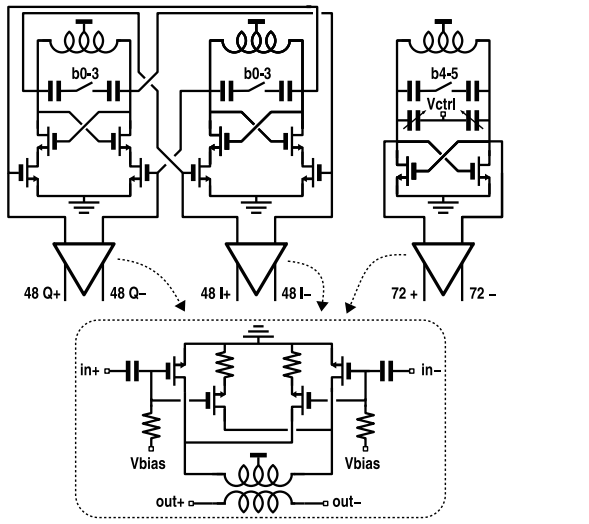

Fig. 11 The implementation of the 48 GHz quadrature VCO (VCO1) (4 bit digital tuning), the 72 GHz differential VCO (VCO2) (analog and
2 bit digital tuning) and their output buffer

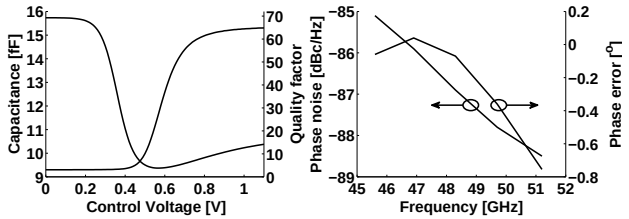

Fig. 12 Simulation results of "VCO1". (a) The capacitance and quality factor as a function of the control voltage of a switched capacitor. (b) The phase noise at 1 MHz offset from the carrier and the quadrature phase error over the tuning range.

tuning range. Also with this set of frequencies, fundamental and harmonic coupling between an on-chip antenna and the VCO is avoided (see fig. 10b). Because the locking range of an LC-VCO is small and no harmonic of VCO1 or VCO2 is close to 120 GHz, there will be no pulling by the 120 GHz modulated output signal. Or interpreted in another way, the sub-harmonics of the output, 40 GHz and 60 GHz, does not fall into the locking range of one of the oscillators.

4 Circuit implementation

The circuit implementation of VCO1, VCO2 and their output buffer is shown in fig. 11. The 48 GHz generation is based on a differential cross-coupled pair oscillator. The oscillation frequency can be tuned using 4 digital switched capacitors, of which the switch is a 41 μm wide transistor with source and drain connected with a large resistor to ground. Figure 12a gives the capacitance and quality factor of a switch over the control voltage range. The simulation results of VCO1 give 4 frequency steps of approximately 1.4 GHz, giving a 5.6 GHz tuning range. Series coupled transistors guarantee the 90 degrees phase shift between both 48GHz oscillators. In comparison with the conventional parallel coupled quadrature oscillators, series coupling results in better phase noise and lower power consumption, but larger parasitic capacitance in the LC-tank [12]. The simulated phase noise and phase error over the tuning range are given in figure 12b.

VCO2 consists of a cross-coupled pair, an inductor, a varactor for analog tuning and two switched capacitors for digital tuning (42.5 μm wide switches). The capacitance and quality factor of the capacitors are given in figure 13a and 13b The tuning range of this oscillator is 11.4 GHz, of which 3.4 GHz is analog controllable and 8 GHz is digital switched. There is a gap of less than 1 GHz between the three analog tuning regions of the VCO. Because VCO1 is also tunable, this gap is closed at the output after mixing VCO1 and VCO2. Figure 13c shows the tuning range and the phase noise of VCO2 as a function of the control voltage of the varactor and the switched capacitors.

For the output buffers a neutralized differential pair is used. The neutralization guarantees stable operation and reverse isolation between the input and the output. At the input, series capacitors are placed to decouple the supply volt-

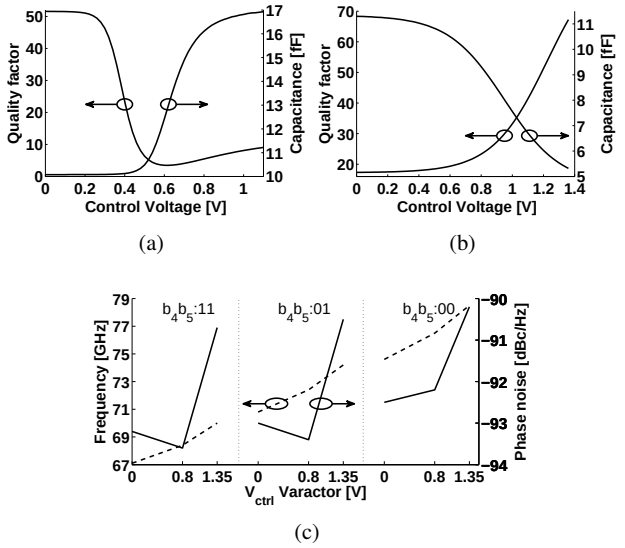

Fig. 13 Simulation results of the 72 GHz VCO. The capacitance and quality factor as a function of the control voltage of (a) a switched capacitor and (b) a varactor. (c) The oscillation frequency and the phase noise at 1 MHz offset from the carrier versus the varactor control voltage

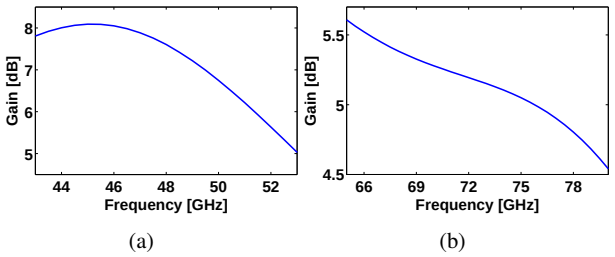

Fig. 14 Simulated large signal power gain of the (a) 48 GHz buffer and (b) 72 GHz buffer

age of the oscillator and the bias voltage of the buffer. A transformer performs a conjugate match between the output of the buffer to input of the next stage, which is the mixer. The small signal power gain of the 48GHz and 72 GHz buffers is 8.8dB and 5dB respectively. The large signal power gain is shown in figure 14. It is seen that the gain at 48 GHz is reduced from 8.8 dB to 7.5 dB due to a large input swing coming from the oscillator.

The generation of the 120 GHz quadrature signals from the 48 GHz and 72 GHz signals is realized with two gilbert cell mixers (for I and Q). Fig. 15 shows the implementation of the mixers. With an input power of -6.5 dBm at 48 GHz and -3 dBm at 72 GHz the differential output power of the mixer at node A and B is -9.5 dBm at 120 GHz. The output of the mixer is matched to the load using a transformer. This tuning also suppresses the 24 GHz mixing product. The output of the mixer is split by a 3-coil transformer to provide

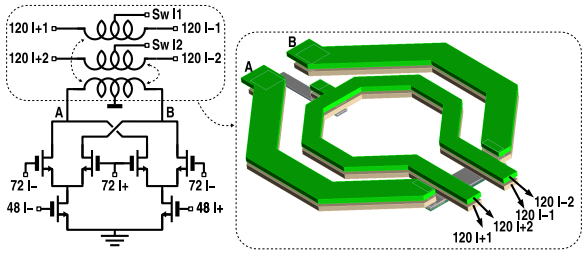

Fig. 15 The implementation of the gilbert cell mixers and the 3-coil output transformer

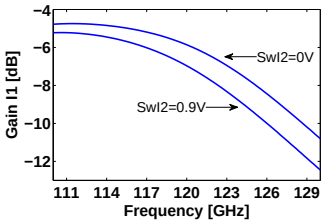

Fig. 16 Gain of the splitter and output buffer $I1$ when the buffer $I2$ is switched on or off

a dual differential output e.g. to send the quadrature LO to both a transmitter and a receiver. In the design of this transformer, advantage is taken of the fact that both top metal layers have the same thickness resulting in a more symmetric layout as shown in fig. 15.

The 120 GHz output of the mixers is buffered with neutralized differential pairs. For switching the buffers on or off, the bias voltages of the gates are connected to the both center taps on the secondary side of the 3-coil transformer. The output buffer is matched to the next building block with transmission lines and transformers. In this test case the one of the outputs ($OutI1$, see fig. 10a) is connected to a probe pad, while the other outputs ($OutI2$ and $OutQ2$) are connected to a downconversion mixer to test the I/Q accuracy. The fourth output ($OutQ1$) is not connected to a load. The gain of the 120 GHz splitter and output buffer $I1$, loaded by the probe pad, is shown in figure 16 for two different simulations. In the first simulation the biasing voltage of the buffer $I2$ is 0 V and in the other simulation this voltage is 0.9 V. From fig. 16 it is clear that that the impdedance matching in the splitter varies when switching on or off the output buffer which is not used. The presented circuit is optimized for the use of only one of both outputs. It can be seen that the output buffer has loss instead of gain and this has a few causes. First, in the splitter there is an inherent loss of 3 dB. To preserve a good I/Q accuracy a symmetrical layout of the matching networks is important, but it makes it harder to obtain a good impedance match. Finally, the routing towards the probe pad requires a long transmission line which also introduces loss.

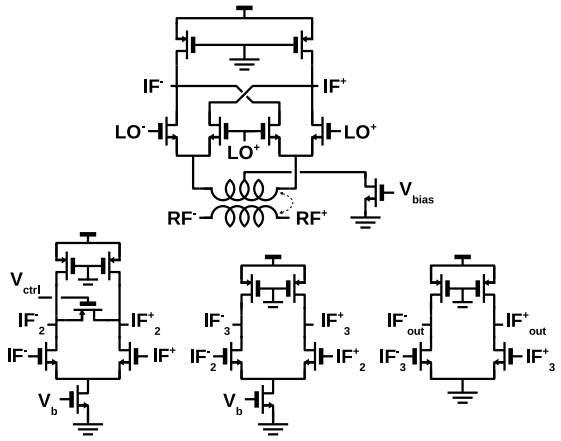

Fig. 17 The implementation of the downconversion mixer and the IF output amplifier

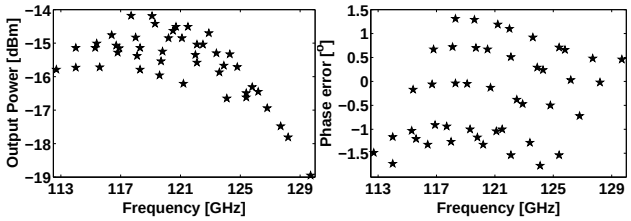

(a) (b)

Fig. 18 Simulation results for (a) output power at the probe pad and (b) phase error at the on-chip downconversoin mixer

The circuits used for measuring the I/Q accuracy are shown in figure 17. An external LO is brought on chip with probes to downconvert the 120 GHz RF signal to an IF output of a few hundreds of MHz. A transmission line is used to match the impedance of the probe pad to the gates of the mixing transistors. The RF signal coming from the output buffer is connected to the sources of the mixing transistors with the help of a transformer. For the biasing of the mixer the center tap of the transformer is used. To be able to drive the load presented by the bondwires and the measurement equipment, an amplifier is put after the mixer. The gain of the first stage of the amplifier can be controlled by the signal V_{ctrl}. The differential voltage gain of the IF amplifier can be tuned from 2.2 to 13 dB in a 100Ω load at a frequency of 400 MHz. The phase error introduced by the downconversion mixer and amplifier is 1 $^\circ$ according to simulations.

To conclude this section, the simulated output power at the probe pad and phase error at the input of the downconversion mixer are presented in figure 18. The different combinations of the control bits of both oscillators and three settings for the varactor control voltage (0 V, 0.8 V, 1.35 V) are simulated. Over the tuning range of 17GHz, the output power varies from -19 to -14.2 dBm and the phase error from -1.8 to +1.3 degrees.

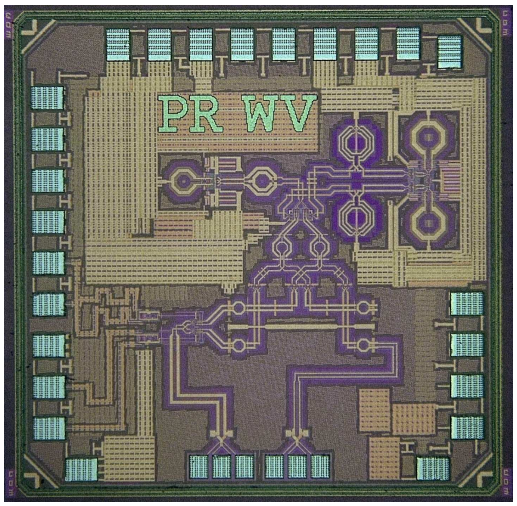

Fig. 19 Die photograph of the chip (1 mm x 1 mm)

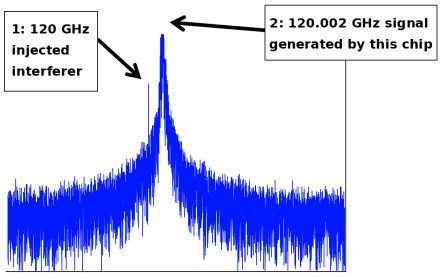

Fig. 20 Spectrum of the output signal of the QVCO. The injected interferer couples into the probe and is also visible in the spectrum. No change in frequency of the oscillator is observed

5 Measurements

The chip is fabricated in a TSMC 45 nm LP CMOS technology with 7 metal layers. A chip photograph is given in fig. 19. The chip size is 1 mm^2 and the core area is 0.2 mm^2. The DC power consumption, including the two VCOs (19 %), buffers (35 %), mixers (22 %) and dual differential output buffers (24 %), is 64 mW.

Intensive sweep measurements by injecting a very close adjacent carrier have been performed and no pulling or spurious generation has been observed for signals around the 120 GHz generated signal. The measurement setup is similar as in fig. 6, but instead of a probe an antenna is used to radiate the interferer towards the chip. As example in fig. 20 a measurement of a -21 dBm injected interferer at an offset of 2 MHz (marker 1) is shown. Both the wanted signal and injected interferer are present at the output of the chip, but no locking or spurious generation occurs. This demonstrates the robustness of the proposed architecture against antenna-VCO coupling.

It is also possible to lock one of the oscillators and measure its locking range at the 120 GHz output. In fig. 21 the spectra of the 120 GHz output signal of the QVCO are

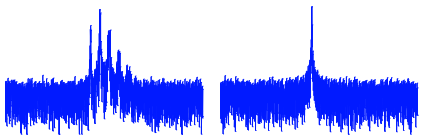

Fig. 21 Measured spectra of the 120 GHz output when VCO2 is pulled by a 72 GHz injected interferer. Two cases are shown: (a) quasi-lock and (b) locked

shown for two cases. In the first case VCO2 is operating in quasi-lock and spurious tones are observed at multiple frequencies. In the second case, VCO2 is locked to the 72 GHz interferer. The phase noise of VCO2 is reduced due to the locking, but the phase noise of VCO1 is still present. Therefore the 120 GHz signal is less pure than the output of the locked VCO in fig. 7.

Similarly it is possible to measure the tuning range of VCO2. This is done by finding the center of the locking range while sweeping the control voltage and the control bits, resulting in a tuning range from 66.6 to 77.5 GHz (fig. 22a). The frequency range of VCO1 is found by sweeping its control bits, measuring the 120 GHz output signal and subtracting the known frequency of VCO2. VCO1 can be tuned from 46.6 to 51.9 GHz (fig. 22b). All the digital control bits are thermometer coded. The results at 120 GHz are shown in fig. 22c. The analog tuning range around the center frequency of 120 GHz is 3.3 GHz. Since the output of VCO2 is always larger than 0.35 V, no excessive voltages are applied across the varactor when the control voltage goes up to 1.35 V. Utilizing the digitally controlled capacitors in both VCO1 and VCO2, the frequency range goes from 113.2 to 129.4 GHz. This means a tuning range of more than 16.2 GHz or 13.5 %. Note that even if the control voltage would be limited to 1 V, the analog tuning is sufficient to overlap the discrete tuning curves.

The output power is measured with an FSU spectrum analyzer and a sub-harmonic mixer and varies from -23 dBm to -30 dBm over the entire frequency range (Fig. 23a). The loss of the measurement setup is removed in this results. The phase noise is measured using the delay-line method of the E5052B signal source analyzer. The phase noise at the center frequency is -87 dBc/Hz and -112 dBc/Hz at 1 MHz and 10 MHz offset, respectively (see fig. 24). The phase noise variations over the tuning range are shown in figure 23b. The 120 GHz signals are also applied to an on-chip down conversion mixer which uses an external LO near 120 GHz. The output of the down conversion mixer is amplified and applied to an oscilloscope. Fig. 25 shows the down converted differential quadrature signals. The measured phase error and I/Q amplitude imbalance are 5 degrees and 0.67dB respectively. These numbers include the errors from the on-chip down conversion mixer and the measurement setup.

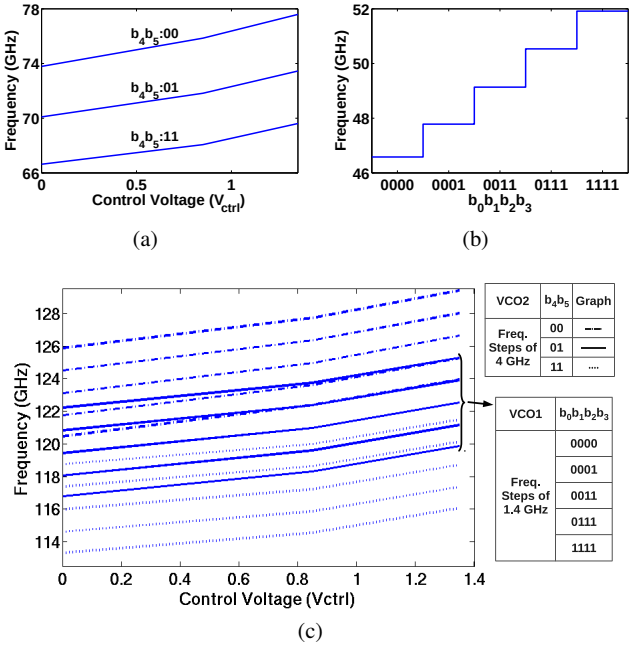

Fig. 22 Measured digital and analog tuning range for (a) VCO2, (b) VCO1 and (c) 120 GHz frequency generator

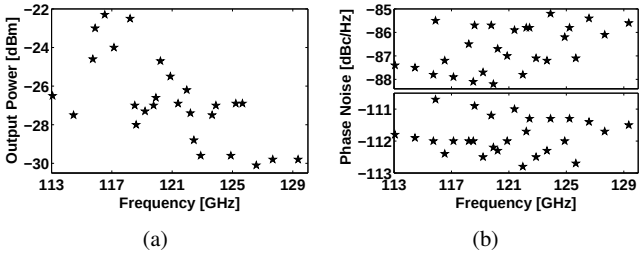

Fig. 23 Measurement results with respect to the operating frequency: (a) output power and (b) phase noise at 1 MHz and 10 MHz offset from the carrier

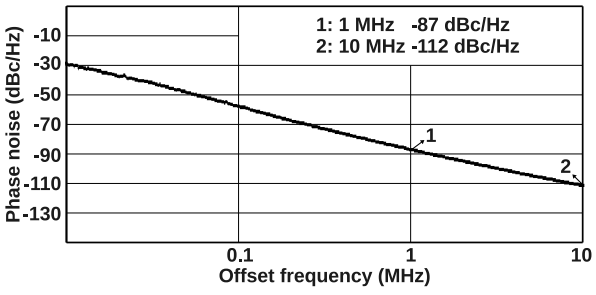

Fig. 24 Measured phase noise at 120 GHz

The results are compared against previous published D-band and mm-wave differential and quadrature VCOs in table 2.

Table 2 *Comparison with previous reported D-band VCOs and mm-wave QVCOs*

Ref	Freq (GHz)	Tuning range (GHz)	Tuning range (%)	L(Δf) (dBc/Hz)	Offset (MHz)	θ_{error} (°)	P_{out} (dBm)	P_{DC} (mW)	Tech	Area (mm^2)	Output Type	FOM[1]
2013 [13]	164.6	9.6	5.8	-73	5	N/A	-13/+1	8/130	65nm	0.1	Single	-119.2
2006 [14]	123	1.6	1.3	-86.4	2	N/A	-14	13.5	90nm	0.19	Diff	-153.2
	140	1.2	0.9	-85.1	2	N/A	-22/-19	9.6	90nm	0.19	Diff	-151.3
2009 [15]	115	5.1	4.4	-85.3	1	N/A	-22.5/-2.5	4.4/19	65nm	0.21	Diff	-170.4
2010 [9]	118.3	9.2	7.8	-83.9	1	N/A	-28.5/-14.2	5.6[2]	65nm	0.22	Diff	-175.7
	122.5	5.28	4.4	-83	1	N/A	-25.3/-20.3	2[2]	65nm	0.22	Diff	-174.6
2011 [16]	58.2	4.35	7.5	-96	1	1.5	N/A	22	65nm	0.075[3]	Quad	-175.4
2013 [17]	55.6	13.5	24.3	-90	1	N/A	N/A	15.6/30	65nm	0.113[3]	Quad	-179.4
2013 [18]	60	0.9	1.5	-95	1	1.2/7	-10	13.3	90nm	0.49	Quad	-162.8
2013 [19]	62.7	10.45	16.6	-94.2	1	0.7	N/A	11.4[2]	65nm	0.039[3]	Quad	-184
2013 [20]	100	4.4	4.4	-110.4	10	1.6	N/A	8.7/21	90nm	0.36	Quad	-173.8
This work	120	16.2	13.5	-87	1	5	-23/-30	64	45nm	1	Quad	-173.1
				-112	10							-178.1

[1] $L(\Delta f) - 20log(f0/\Delta f \cdot FTR/10) + 10log(P_{DC})$

[2] Output buffers not included

[3] Only core area

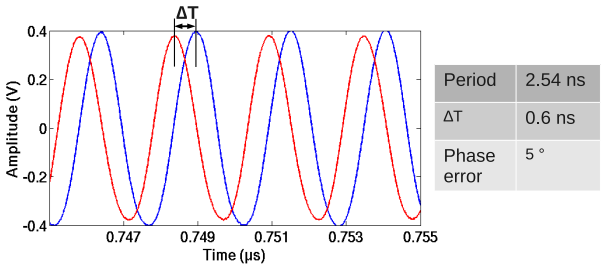

Fig. 25 Measured phase error of the downconverted I/Q signals

6 Star QAM Transmitter

The measurements in the previous section prove immunity against pulling by an external signal. To further test the performance of the presented frequency generator, it is also integrated together with a modulator, a power amplifier and a bondwire antenna. The design of the complete transmitter is described in [3]. The tuning range of the oscillator was large enough to align the oscillation frequency with the operating frequency of the transmitter. Also, the output power was large enough to drive de modulator. As a result data rates up to 10 Gbps could be transmitted and this without any performance degradation of antenna-VCO pulling.

7 Conclusion

LO pulling in a QPSK transmitter is analysed and appears to severly degrade the purity of the LO generation. As a solution, a 120 GHz quadrature oscillator is presented. By muliplying the output signals of two independent oscillators, quadrature generation and large tuning range becomes feasible at 120 GHz. Another major advantage of the architecture is that the output signal is not harmonically related to both oscillators, which enables integration with on-chip antennas. A record tuning range of 16.2 GHz (13.3 %) and a phase noise of -112 dBc/Hz at 10 MHz offset is measured.

Acknowledgements The research leading to these results has received funding from the European Research Council under the European Union's Seventh Framework Program (FP/2007-2013) / ERC Grant Agreement n. 227680. The authors want to thank NXP Research Eindhoven for supporting this research.

References

1. W. Volkaerts, M. Steyaert, and P. Reynaert. (2013). A 120GHz quadrature frequency generator with 16.2GHz tuning range in 45nm CMOS. *IEEE Radio Frequency Integrated Circuits Symposium (RFIC)*. 207–210.
2. N. Deferm and P. Reynaert. (2013). Design, implementation and measurement of a 120 GHz 10 Gb/s phase-modulating transmitter in 65 nm LP CMOS. *Analog Integrated Circuits and Signal Processing*. DOI 10.1007/s10470-013-0027-9.
3. N. Deferm, W. Volkaerts, J. F. Osorio, A. de Graauw, M. Steyaert, and P. Reynaert. (2013). A 120GHz Fully integrated 10 Gbps Wireless transmitter with On-chip Antenna in 45nm LP CMOS. *IEEE European Solid-State circuits Conference (ESSCIRC)*. 331–334.
4. M. Tytgat and P. Reynaert. (2013). A plastic waveguide receiver in 40nm CMOS with on-chip bondwire antenna. *IEEE European Solid-State circuits Conference (ESSCIRC)*. 335–338.
5. S. Bronckers, G. Vandersteen, L. De Locht, M. Libois, G. Van der Plas, and Y. Rolain. (2009). Experimental Analysis of the Coupling Mechanisms Between a 4 GHz PPA and a 5 GHz LC -VCO. *IEEE*

Transactions on Instrumentation and Measurement, 58(8). 2706–27139.
6. R. Adler. (1973). A study of locking phenomena in oscillators. *Proceedings of the IEEE*. 61(10). 1380–1385.
7. B. Razavi. (2004). A study of injection locking and pulling in oscillators. *IEEE Journal of Solid-State Circuits*. 39(9). 1415–1424.
8. C.-H. Hsiao, C.-T. Chen, T.-S. Horng, and K.-C. Peng. (2012). Design of a Direct Conversion Transmitter to Resist Combined Effects of Power Amplifier Distortion and Local Oscillator Pulling. *IEEE Transactions on Microwave Theory and Techniques*. 60(6). 2000–2009.
9. W. Volkaerts, M. Steyaert, and P. Reynaert. (2011). 118GHz fundamental VCO with 7.8% tuning range in 65nm CMOS. *IEEE Radio Frequency Integrated Circuits Symposium (RFIC)*. 1–4.
10. N. Deferm and P. Reynaert. (2010). A 120GHz 10Gb/s phase-modulating transmitter in 65nm LP CMOS. *IEEE International Solid-State Circuits Conference Digest of Technical Papers (ISSCC)*. 290–292.
11. C.-H. Hsiao, C.-J. Li, F.-K. Wang, T.-S. Horng, and K.-C. Peng. (2010). Analysis and Improvement of Direct-Conversion Transmitter Pulling Effects in Constant Envelope Modulation Systems. *IEEE Transactions on Microwave Theory and Techniques*. 58(12). 4137–4146.
12. P. Andreani and X. Wang. (2004). On the phase-noise and phase-error performances of multiphase LC CMOS VCOs. *IEEE Journal of Solid-State Circuits*. 39(11). 1883–1893.
13. B. Khamaisi and E. Socher. (2013). A 159 - 169 GHz frequency source with 1.26 mW peak output power in 65 nm CMOS. *European Microwave Integrated Circuits Conference (EuMIC)*. 536–539.
14. C. Cao and K. O. (2006). A 140-GHz fundamental mode voltage-controlled oscillator in 90-nm CMOS technology. *IEEE Microwave and Wireless Components Letters*. 16(10). 555–557.
15. W. Badalawa, S. Lim, and M. Fujishima. (2009). 115GHz CMOS VCO with 4.4% tuning range. *European Microwave Integrated Circuits Conference (EuMIC)*. 128 –131.
16. U. Decanis, A. Ghilioni, E. Monaco, A. Mazzanti, and F. Svelto. (2011). A mm-Wave quadrature VCO based on magnetically coupled resonators. *IEEE International Solid-State Circuits Conference Digest of Technical Papers (ISSCC)*. 280–282.
17. L. Wu and H. Luong. (2012). A 49-to-62GHz CMOS quadrature VCO with bimodal enhanced magnetic tuning. *IEEE European Solid-State circuits Conference (ESSCIRC)*. 297–300.
18. C.-H. Lin, Y.-C. Liu, Y.-L. Yeh, H.-C. Chiu, and H.-Y. Chang. (2013). A 60-GHz low DC power self-injection coupling CMOS quadrature voltage-controlled oscillator with high quadrature accuracy. *IEEE MTT-S International Microwave Symposium Digest (IMS)*. 1–3.
19. X. Yi, C. C. Boon, H. Liu, J. F. Lin, J. C. Ong, and W. M. Lim. (2013). A 57.9-to-68.3GHz 24.6mW frequency synthesizer with in-phase injection-coupled QVCO in 65nm CMOS. *IEEE International Solid-State Circuits Conference Digest of Technical Papers (ISSCC)*. 354–355.
20. K.-T. Lin, H.-K. Chen, and S.-S. Lu. (2013). 100 GHz transformer-coupled quadrature oscillator. *Electronics Letters*. 49(4). 266–267.